

Thermal Enhanced Adaptive Interval Estimation in Battery Packs with Heterogeneous Cells*

Dong Zhang¹, Luis D. Couto², Preet Gill¹, Sebastien Benjamin³, Wenteng Zeng⁴, and Scott J. Moura¹

Abstract—The internal states of Lithium-ion batteries need to be carefully monitored during operation to manage energy and safety. In this paper, we propose a thermal enhanced adaptive interval observer for state of charge (SOC) and temperature estimation for a battery pack. For a large battery pack with hundreds or thousands of heterogeneous cells, each individual cell characteristic are different from others. Practically, applying estimation algorithms on each and every cell would be mathematically and computationally intractable, **since battery packs are often characterized by combinations of differential equations (state dynamics) and algebraic constraints (Kirchhoff's laws)**. These issues are tackled using an interval observer based on monotone/cooperative system theory, whose novelty lies in considering cell heterogeneity as well as state-dependent parameters as unknown, but bounded uncertainties. The resulting interval observer maps the bounded uncertainties to a feasible set of SOC and temperature estimation for all cells in the pack at each time instant. **The present work addresses the significant conservatism under extreme conditions with large currents via a thermal enhanced adaptive scheme.** The proposed interval estimation is scalable and computationally tractable since it is independent of the number of cells in a pack, as numerically demonstrated in a comparison with respect to a state-of-the-art single cell state observer. Stability and inclusion of the adaptive interval observer are proven and validated through simulations.

I. INTRODUCTION

Lithium-ion (Li-ion) batteries play a key role in achieving energy sustainability and reduction in greenhouse gas emissions. Li-ion batteries benefit from high energy density, which has motivated their wide use in a variety of applications including electric vehicles (EV) and grid energy storage. In recent years, a substantial body of research on real-time control and estimation algorithms for batteries has emerged. However, safe and efficient operation of battery packs remains a challenge, especially as the performance requirements of these devices increase.

Large-scale energy storage systems require hundreds to thousands of cells connected in series and parallel to achieve demanded power and voltage [1]. A battery pack's instantaneous power capability is crucial for on-board management and safe operation [2]. An advanced battery management

system (BMS) implements real-time control/estimation algorithms to enhance battery performance while improving safety. One of the most crucial functions of a BMS is to perform state of charge (SOC) estimation. However, real-time SOC estimation for a pack is a very intricate task due to (i) limited sensing and measurements, (ii) complex electrochemical-thermal-mechanical physics, and (iii) high computational cost [3].

To date, different battery models oriented towards state and parameter estimator designs for single battery cell have been extensively proposed in the literature, which can be classified into electrochemical white box (first principle) models [4], [5], [6], [7], [8], equivalent-circuit gray box models [9], [10], [11], [12] and data-driven black box models [13], [14], [15]. Electrochemical models describe the diffusion, thermodynamics, and electrochemical kinetics. Even though these models can predict the internal states with high accuracy, e.g., lithium concentrations and over-potentials, their associated complex mathematical structure makes the design of online estimators from these models intractable. Consequently, most estimator design approaches are constructed based on reduced-order electrochemical models [16], [17]. On the other hand, data-driven models normally demand a significant amount of training data to predict the input-output behavior of battery systems, which suffers from low physical interpretability. Although each modeling framework has its merits and drawbacks, equivalent circuit models (ECM) provide a reasonable trade-off between model complexity and prediction accuracy [9] with idealized physical elements such as resistors and capacitors. ECMs can be made more accurate by increasing the system order to account for additional electrochemical phenomena [18].

An important fact often ignored during battery equivalent circuit modeling is the time-varying electrical parameters. In practice, internal parameters, e.g. resistances and capacitances, are non-linearly dependent on the cell's temperature and SOC, motivating the inclusion of thermal dynamics in the model. In fact, in addition to causing potential battery safety issues [19], thermal effects have also been shown to be key factors in the rate of battery degradation [20], [21]. Among existing battery thermal models, high-fidelity thermal models have more accurate predictions, but suffer from high computational cost, rendering them of little use for on-board thermal management [22]. First principles-based two-state thermal model for the cell's core and surface temperatures provide a balanced trade-off between computational efficiency and fidelity [23]. Coupled equivalent circuit-thermal models with temperature dependent parameters have been studied and used for state estimation via an adaptive observer in [24].

With the aforementioned battery cell modeling strategies, battery pack modeling approaches can typically be divided

*This work is sponsored by Total S.A. and Saft S.A..

¹Dong Zhang, Preet Gill, and Scott J. Moura are with Department of Civil and Environmental Engineering, University of California, Berkeley, California, 94720, USA. {dongzhr, preetgill77, smoura}@berkeley.edu

²Luis D. Couto is with Department of Control Engineering and System Analysis, Université Libre de Bruxelles, B-1050 Brussels, Belgium. lcoutome@ulb.ac.be. He would like to thank the Wiener-Anspach Foundation for its financial support.

³Sebastien Benjamin is with Saft S.A.. Sebastien.BENJAMIN@saftbatteries.com

⁴Wenteng Zeng is with Total S.A.. wenteng.zeng@total.com

into three categories. The first approach treats the entire pack as one lumped single cell [25]. However, the internal states of individual cells within the pack are often different, due to heterogeneities arising from parametric uncertainties and differences in cell aging levels [26]. Therefore, some cells are more prone to violate safety-critical constraints than others, which cannot be resolved from the lumped single cell approach. The second modeling approach also relies on a single cell model, but it focuses on a set of specific in-pack cells – the weakest and the strongest ones, as representatives of the pack dynamics [27], [28]. The last modeling approach is based on the interconnection of single cell models [26], [29], [30]. This approach benefits from high fidelity with cell-by-cell resolution, but it suffers from high real-time computational burden. Existing techniques for battery pack state estimation include Luenberger observers [31], Kalman filters (KF) [32], unscented Kalman filters [33], and sliding mode observers [34], among others. However, all the previously mentioned techniques require a state observer for each cell, which becomes computationally intractable for large packs.

In the aforementioned stochastic filtering framework (e.g., variations of Kalman filters), the process and measurement noises are often assumed to be Gaussian. The system characteristics, i.e. mean and variance, are required by filtering algorithms. Nevertheless, the statistical and calibration procedures to obtain these characteristics are often tedious [35]. In contrast, interval estimation, *a.k.a.* bounded error or the set-membership estimation approach, assumes that the measurement and process noises are unknown but bounded – requiring no information on the statistical distributions of the model uncertainties [35], [36], [37]. Specifically, a state interval observer seeks to derive a feasible set for the unknown/unmeasured states and map the bounded uncertainties to the state intervals at every time instant. In a battery pack with hundreds or thousands of cells, designing and executing state estimation algorithms based on highly nonlinear and coupled dynamics for every single cell in real time becomes intractable. The interval observer benefits from its scalability by deriving only mathematically guaranteed upper and lower bounds that enclose all unmeasured internal states for all cells in a pack. That is, the computational complexity of an interval observer is independent of the number of cells in a pack. Previously, only Perez *et al.* examined a sensitivity-based interval observer for single cell SOC estimation from an electrochemical perspective [38], but did not provide provable observer stability and inclusion properties.

In this work, we advance our preliminary work in [39] by proposing a thermal enhanced interval observer for SOC estimation in battery packs for a string of cells. This article’s main contributions against our previous work [39] are summarized as follows:

- The interval observer design is calibrated and enhanced by the pack’s thermal response (more details in Fig. 5). This significantly eliminates design conservatism in [39] and effectively renders improved estimation accuracy under extreme conditions with large applied currents.
- Rigorous demonstration of the practical implementation improvements via a comparison study with respect to the

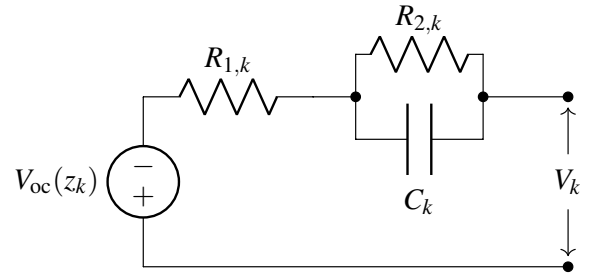


Fig. 1. The schematic of an equivalent circuit model for a single cell.

state-of-the-art extended Kalman filter (EKF).

- The study is carried out on a string of cells (or a string of parallel modules), which represents a much wider and general class of topology in a pack. **The previous study in [39] only considers parallel-connected cells.**

The remainder of this paper is organized as follows. A coupled electro-thermal model is developed in Section II, for a battery pack with cells connected in series. Next, a brief motivation of the problem is presented in Section III. For the reader’s convenience, interval observer preliminaries are given in Section IV. The observer design for the battery pack is pursued in Section V, and followed by a **numerical** assessment of its performance in Section VI. Conclusions and future works are discussed in Section VII.

Notation. Throughout the manuscript, the symbols I_n denotes the identity matrix with dimension $n \times n$. For a matrix $A \in \mathbb{R}^{n \times n}$, $\|A\|_{\max} = \max_{i,j=1,2,\dots,n} |A_{i,j}|$ (the element-wise maximum norm). The relation $Q \succ 0$ ($Q \prec 0$) means that the matrix $Q \in \mathbb{R}^{n \times n}$ is positive (negative) definite. We denote as \mathcal{L}_{∞} the set of all x with $\|x\| \leq \infty$, where $\|\cdot\|$ is the infinity norm. The inner product between $x, y \in \mathbb{R}^n$ is given by $\langle x, y \rangle = \sum_{i=1}^n x_i y_i$. For vectors $x_1, x_2 \in \mathbb{R}^n$ and matrices $A_1, A_2 \in \mathbb{R}^{n \times n}$, the relations $x_1 \leq x_2$ ($x_1 \geq x_2$) and $A_1 \leq A_2$ ($A_1 \geq A_2$) denote element-wise less (greater) than or equal. For a matrix $A \in \mathbb{R}^{n \times n}$, define $A^+ = \max\{0, A\}$ and $A^- = A^+ - A$. For a vector $x \in \mathbb{R}^n$, define $x^+ = \max\{0, x\}$ and $x^- = x^+ - x$.

II. MODEL DEVELOPMENT

This section reviews an equivalent-circuit model coupled with a two-state thermal model for a single battery cell, which is then electrically and thermally interconnected with other cell models to form a series arrangement of cells. It is noteworthy that although the estimation algorithm development in this work is based on equivalent circuit type models, this framework could be generalized to battery packs characterized by other models, e.g., electrochemical models.

A. Single Battery Cell

The ECM for a single cell k ($k = 1, 2, \dots$), consisting of an open circuit voltage (OCV) in series connection with an

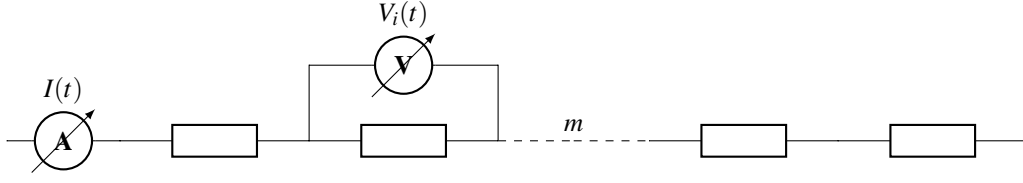


Fig. 2. A battery pack configuration with m heterogeneous cells (or parallel modules) connected in series. Cell (module) current and local voltages and temperatures can be measured, but only the maximum and minimum values are accessible to BMS algorithms. See Assumption 1.

ohmic resistance and an $R-C$ pair in parallel, is shown in Fig. 1 and mathematically described by

$$\dot{z}_k(t) = \frac{1}{Q_k} I_k(t), \quad (1)$$

$$\dot{V}_{c,k}(t) = -\frac{1}{R_{2,k}(z_k, T_k) C_k(z_k, T_k)} V_{c,k}(t) + \frac{1}{C_k(z_k, T_k)} I_k(t), \quad (2)$$

$$V_k(t) = V_{oc}(z_k(t)) + V_{c,k}(t) + R_{1,k}(z_k, T_k) I_k(t), \quad (3)$$

where $z_k(t)$ represents the SOC for the k -th cell, T_k is the cell temperature (to be defined), and $V_{c,k}(t)$ denotes the relaxation voltage across the $R_{2,k}-C_k$ pair. Symbol $R_{1,k}$ is an ohmic resistance. Moreover, $I_k(t)$ is the current, and the convention is maintained such that positive current is charging and negative current indicates discharging. The electrical model parameters, namely $R_{1,k}$, $R_{2,k}$, and C_k , are dependent on cell SOC and temperature, and such dependency can be explicitly characterized via an offline experimental procedure. For instance, for a LiFePO₄/Graphite cell, it is observed that $R_{1,k}$ has minimal dependence on SOC and strong dependence on temperature, and its value decreases as the temperatures rises [40]. The temperature dependence in general follows an Arrhenius-like behavior. Moreover, $R_{2,k}$ and C_k have notable dependence on both SOC and temperature. The output equation (3) for the k -th cell provides the voltage response characterized by a nonlinear open circuit voltage (V_{oc}) as a function of SOC, relaxation voltage from the $R_{2,k}-C_k$ pair, and voltage associated with the resistance $R_{1,k}$.

A two-state thermal model for a cylindrical cell is adopted for the dynamics of core and surface temperatures [40]. However, in a battery pack, the cells are thermally coupled through coolant flow and heat exchange with adjacent cells. These effects are modeled by the following dynamical system for the k -th cell in the pack [41]:

$$C_{c,k} \dot{T}_{c,k}(t) = \dot{q}_k(t) + \frac{T_{s,k}(t) - T_{c,k}(t)}{R_{c,k}}, \quad (4)$$

$$C_{s,k} \dot{T}_{s,k}(t) = \frac{T_{f,k}(t) - T_{s,k}(t)}{R_{u,k}} - \frac{T_{s,k}(t) - T_{c,k}(t)}{R_{c,k}} + \frac{T_{s,k-1}(t) + T_{s,k+1}(t) - 2T_{s,k}(t)}{R_{cc}}, \quad (5)$$

$$\dot{q}_k(t) = I_k(t) [V_k(t) - V_{oc}(z_k(t))], \quad (6)$$

$$T_k(t) = \frac{1}{2} (T_{s,k}(t) + T_{c,k}(t)), \quad (7)$$

where $T_{c,k}$ and $T_{s,k}$ are the core and surface temperatures for the k -th cell. Symbols $R_{c,k}$, $R_{u,k}$, $C_{c,k}$, and $C_{s,k}$ represent heat conduction resistance between core and surface, convection resistance between ambient and surface, core heat capacity,

and surface heat capacity, respectively. Herein, $C_{c,k}$ and $C_{s,k}$ depend on the cell material thermal properties and the mass of the rolled electrode assembly and the casing of a cylindrical cell [23], [42]. Meanwhile, $R_{u,k}$ is affected by the coolant flow rate. Additionally, $R_{c,k}$ can be computed from the conductivity and dimensions of the wound cell electrode assembly and cell casing, and contact thermal resistance between electrodes and the casing [23]. Symbol $\dot{q}_k(t) \geq 0$ is the internal heat generation rate including joule heating and energy dissipated by electrode over-potentials. Moreover, in (5), the heat conduction between adjacent cells is modeled as heat flow over conduction resistance R_{cc} , which is driven by the surface temperature differences between the cells. In this work, the coolant flow temperature $T_{f,k}$ at cell k is assumed uniform across all cells and will be simply denoted by T_f subsequently. For each cell k , the average temperature between core and surface is represented by T_k in (7), which is the temperature used to schedule the parameters in (1)-(3). It is worth noting that the electrical model (1)-(3) and the thermal model (4)-(7) are coupled via $\dot{q}_k(t)$ and parameters R_1 , R_2 , and C in a nonlinear fashion.

The measured quantities for the coupled electro-thermal model (1)-(7) are the cell voltage and surface temperature:

$$y_k(t) = [V_k(t), T_{s,k}(t)]^\top. \quad (8)$$

B. Series Arrangement of Battery Cells

When battery cells are connected in series (Fig. 2), all cells share the same input current according to Kirchhoff's current law. In this study, we consider the scenario where the cells are heterogeneous. Namely, they may have different model parameters (cell capacity, internal resistance etc.), different SOC levels, and different temperature distribution. The above-mentioned heterogeneity among cells can be caused by manufacturing, temperature variability along the string, and battery degradation [43]. Results from [44], [45] even show that there exists considerable variability for batteries manufactured from the same procedure. For a string of m cells in series, the overall voltage supplied by the string is given by

$$V(t) = \sum_{k=1}^m V_k(t). \quad (9)$$

We are now positioned to make the following assumption on the hardware sensing of the battery string, oriented towards an interval state estimation design.

Assumption 1. The current, voltage, and surface temperature of every cell in the string, i.e. $I_k(t)$, $V_k(t)$, and $T_{s,k}(t)$, $\forall k \in$

$\{1, 2, \dots, m\}$, are measurable. However, only the maximum output signals $V_{\max}(t)/T_{s,\max}(t)$ and minimum output signals $V_{\min}(t)/T_{s,\min}(t)$ across all cells in the pack at every time instant t are accessible by the BMS estimation algorithms, where

$$V_{\max}(t) = \max_{k=1,2,\dots,m} V_k(t), \quad \forall t > 0, \quad (10)$$

$$V_{\min}(t) = \min_{k=1,2,\dots,m} V_k(t), \quad \forall t > 0, \quad (11)$$

$$T_{s,\max}(t) = \max_{k=1,2,\dots,m} T_{s,k}(t), \quad \forall t > 0, \quad (12)$$

$$T_{s,\min}(t) = \min_{k=1,2,\dots,m} T_{s,k}(t), \quad \forall t > 0. \quad (13)$$

In spite of Assumption 1, however, we do not assume that the extreme values of $V_k(t)$ or $T_{s,k}$ will come from the same cells throughout the battery charging/discharging. A typical battery pack has the hardware and power to monitor in real time the local voltage of every cell to prevent cell overcharging, over-discharging, and safety issues. Nonetheless, executing a single cell based estimation and control algorithm using local measurements would require a massive amount of computing power and is impractical, no matter if the computer is placed in a centralized cloud or in a decentralized manner. Furthermore, the traffic on the communication buses that are used to transfer the measured local data to the cloud or the centralized computer oftentimes is heavy due to the large number of cells and bandwidth limits, prohibiting the data transfer in an aggregated fashion. These facts motivate the usage of only the extreme values of voltage measurements. Practically, the cells that provide extreme voltage values are also the representations of the best and worst cells in a pack.

III. MOTIVATION

Even though the focus of this manuscript is on cells in series, we illustrate in this section the heterogeneity for cells in both series and parallel configurations via open-loop simulation studies. Without loss of generality, we consider two LiNiMnCoO₂/Graphite (NMC) type cells with 2.8 Ah nominal capacity. In this embodiment, the cells have identical SOC-OCV relationship, and the heterogeneity arises from:

- Difference in SOC initialization.
- Difference in electrical parameters due to SOC and temperature variations.
- Unevenly distributed currents due to parameter variation (applies to parallel case only).
- Difference in temperature due to current variation (applies to parallel case only).

A transient electric vehicle-like charge/discharge cycle generated from the urban dynamometer driving schedule (UDDS) is applied. Specifically, for the parallel case, the total applied current (summation of local currents) is plotted in Fig. 3(a). The current applied to the series case is appropriately scaled and shown in Fig. 4(a).

Figures 3 and 4 portray the cases for cells in parallel and series, respectively. In both cases, the cells are initialized with different SOC. In the case of the parallel arrangement in Fig. 3, it can be observed that even though the applied total current is small initially (around zero, see Fig. 3(a)), Cell 1

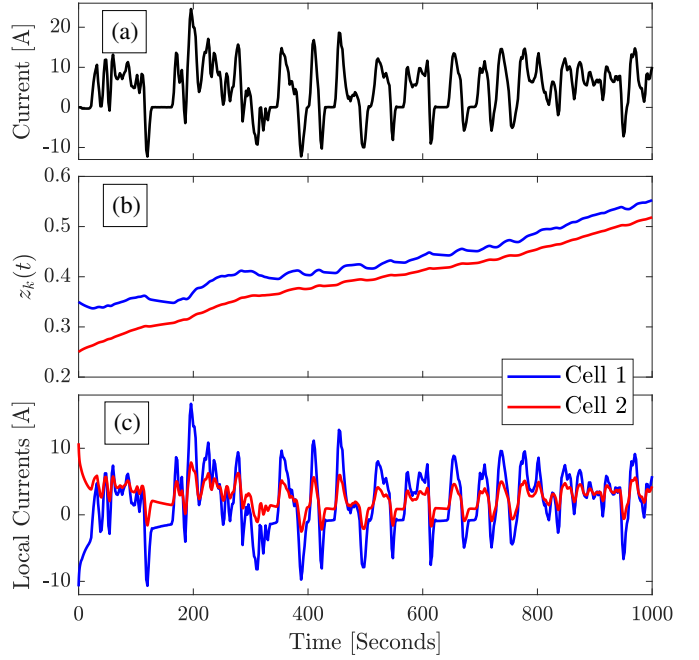


Fig. 3. Simulation results of two cells in parallel using coupled electro-thermal dynamics with temperature and SOC dependent electrical parameters. In (b)-(c), cells are initialized at different SOCs. The total current distributes unevenly due to both parameter and initialization heterogeneities.

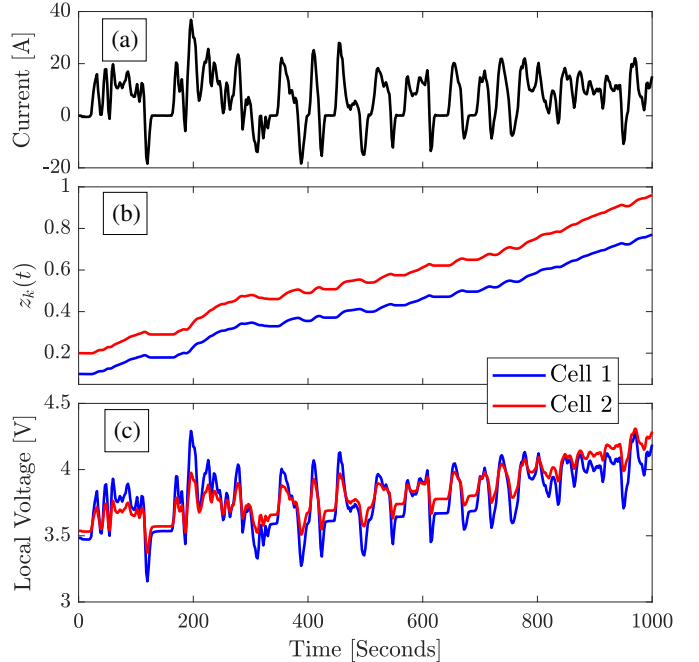


Fig. 4. Simulation results of two cells in series using coupled electro-thermal dynamics with temperature and SOC dependent electrical parameters. In (b)-(c), the initial cell SOCs are distinct. This discrepancy will persist because all cells accept the same input current.

takes a large negative current (around -10 A) and Cell 2 positions itself at a large positive current (around $+10$ A). This occurs because $z_1(0)$ is initialized higher (see 3(b)). In such cases, notice how single cells can be violating safety constraints (e.g. maximum current, see Fig. 3(c)) but the pair

of parallel cells is not, whereas the latter is the one that is often supervised. In the long run, however, the values for z follow a similar trend while seemingly approaching. This behaviour can be ascribed to the parallel connection that forces a natural voltage balance, and not SOC balance, between the cells. In the more extreme and realistic situations where the cells are completely different, i.e. in terms of OCVs and parameters, the SOCs never converge and cells accept different current rates, which promote different aging patterns and increase cell-to-cell variation in positive feedback. The case of the series arrangement shown in Fig. 4, where cell 1 has a higher internal resistance, can be considered as a milder scenario compared to the parallel case in terms of current behaviour (see Fig. 4(c)). However, SOC discrepancy is worse and more persistent in time (see Fig. 4(c)), since the z values for the two cells will never synchronize – a bias will always exist – unless an external active action is taken, such as cell balancing.

In a battery pack composed of hundreds or thousands of heterogeneous cells, executing state estimation algorithms in real time based on a highly nonlinear and coupled model consists of differential-algebraic equations accounting for every single cell in the pack is intractable and not scalable. This motivates our subsequent study on interval observers to increase algorithm scalability and reduce computation and design complexity.

IV. INTERVAL OBSERVER BACKGROUND

The development of finite-dimensional interval observers based on monotone system theory closely follows the work in [35], [36], [37]. In this section, we discuss the preliminaries and provide theoretical insights.

Consider the following nonlinear model dynamics [37]:

$$\dot{x} = f(x) + B(\theta)u + \delta f(x, \theta), \quad x(0) = x_0, \quad (14)$$

$$y = h(x) + \delta h(\theta)u, \quad (15)$$

where $x \in \mathbb{R}^n$ is the state vector, and $u \in \mathbb{R}$ and $y \in \mathbb{R}$ are the system input and output, respectively. The considered system is a single-input-single-output (SISO) type. The functions $f(x)$ and $h(x)$ are deterministic and smooth, and δf is uncertain and assumed to be locally Lipschitz continuous with respect to x . It is noted that the nominal terms $f(x)$ and $h(x)$ can be freely assigned by the designer via the modification of δf and δh . The parameter vector θ is unknown and potentially state-dependent and time-varying. Suppose that the values of the uncertain parameter vector θ are not available for measurements, and only the set of admissible values Θ is known, where $\theta \in \Theta \subset \mathbb{R}^p$ and p denotes the number of uncertain parameters in the model. The initial conditions of the states belong to a compact set $x_0 \in [\underline{x}_0, \bar{x}_0]$, where \underline{x}_0 and \bar{x}_0 are given. The objective of the interval observer is to design a system with state vector $\bar{x}(t)$ and $\underline{x}(t)$ such that

$$\underline{x}(t) \leq x(t) \leq \bar{x}(t), \quad \forall t > 0, \quad (16)$$

and $\bar{x}, \underline{x} \in \mathcal{L}_\infty^n$.

A. Preliminaries

Interval observer designs in literature builds on the properties of cooperative (monotone) systems. A matrix $A \in \mathbb{R}^{n \times n}$ is Hurwitz if all its eigenvalues are located in the left half of the complex plane. It is Metzler if all off-diagonal elements are non-negative. Any solution of the system

$$\dot{x}(t) = Ax(t) + w(t), \quad (17)$$

where $w(t)$ is not necessarily linear, with $x \in \mathbb{R}^n$, and a Metzler matrix $A \in \mathbb{R}^{n \times n}$, is element-wise non-negative for all $t \geq 0$, provided that $w(t) \in \mathbb{R}_+^n$, $\forall t \geq 0$, and $x(0) \geq 0$ [46]. System (17) is also known as an internally positive system [47].

Lemma 1 ([36]). *Let $x \in \mathbb{R}^n$ be a vector variable and $\underline{x} \leq x \leq \bar{x}$ for some $\underline{x}, \bar{x} \in \mathbb{R}^n$. Let $A \in \mathbb{R}^{n \times n}$ be a matrix variable, and $\underline{A} \leq A \leq \bar{A}$ for some $\underline{A}, \bar{A} \in \mathbb{R}^{n \times n}$. Then*

$$\begin{aligned} \underline{A}^+ \underline{x}^+ - \bar{A}^+ \underline{x}^- - \underline{A}^- \bar{x}^+ + \bar{A}^- \bar{x}^- \\ \leq Ax \leq \\ \bar{A}^+ \bar{x}^+ - \underline{A}^+ \bar{x}^- - \bar{A}^- \underline{x}^+ + \underline{A}^- \underline{x}^-. \end{aligned} \quad (18)$$

B. Model Coordinate Transformation

One can obtain a nominal system of (14)-(15) by setting $B = 0$, $\delta f = 0$, and $\delta h = 0$,

$$\dot{x} = f(x), \quad (19)$$

$$y = h(x). \quad (20)$$

According to [35], [48], a time-varying nonlinear and invertible state transformation, based on the Lie derivatives, yields a partial-linear dynamics in the new state coordinate. Denote the gradient of a scalar field h by dh , and the Lie derivative of h along a vector field f is given by the inner product $L_f h(x) = \langle dh(x), f(x) \rangle$. High-order Lie derivatives are computed with the iteration $L_f^k h(x) = L_f(L_f^{k-1} h(x))$ where $L_f^0 h(x) = h(x)$. The nominal system (19)-(20) is locally observable around $x = x_e$ if the observability matrix

$$\mathcal{O}(x_e) = \begin{bmatrix} dh(x_e) & dL_f h(x_e) & \cdots & dL_f^{n-1} h(x_e) \end{bmatrix}^\top \quad (21)$$

has full rank, i.e., $\text{rank}(\mathcal{O}) = n$. Under this scenario, the row vectors $dh, dL_f h, \dots, dL_f^{n-1} h$ are linearly independent and the vectors $h(x), L_f h(x), \dots, L_f^{n-1} h(x)$ form the new coordinate for the states in a neighborhood of $x = x_e$ defined by

$$\Phi(x) = \begin{bmatrix} \phi_1(x) \\ \phi_2(x) \\ \vdots \\ \phi_n(x) \end{bmatrix} = \begin{bmatrix} h(x) \\ L_f h(x) \\ \vdots \\ L_f^{n-1} h(x) \end{bmatrix}, \quad (22)$$

and the transformation map $\xi = \Phi(x)$ defines a local diffeomorphism, where a diffeomorphism is known as a continuously differentiable map with a continuously differentiable inverse. Thus the inverse transformation $x = \Phi^{-1}(\xi)$ is well defined. Using this diffeomorphism, the nominal system (19)-(20) can be written as

$$\dot{\xi} = \tilde{A}\xi + \tilde{b}\varphi(\xi), \quad (23)$$

$$y = \tilde{C}\xi, \quad (24)$$

where

$$\tilde{A} = \begin{bmatrix} 0 & 1 & 0 & \cdots & 0 \\ 0 & 0 & 1 & \cdots & 0 \\ \vdots & \vdots & \ddots & \ddots & \vdots \\ 0 & 0 & 0 & \cdots & 1 \\ 0 & 0 & 0 & \cdots & 0 \end{bmatrix}, \quad (25)$$

$$\tilde{b} = \begin{bmatrix} 0 & \cdots & 0 & 1 \end{bmatrix}^\top, \quad (26)$$

$$\tilde{C} = \begin{bmatrix} 1 & 0 & \cdots & 0 \end{bmatrix}, \quad (27)$$

$$\varphi(\xi) = L_f^n h(x)|_{x=\Phi^{-1}(\xi)}. \quad (28)$$

The coordinate transformation obtained from the locally observable nominal system (19)-(20) is then utilized to transform the original uncertain system (14)-(15) into a partial-linear expression:

$$\dot{\xi} = A_0 \xi + \delta A(\theta) \xi + b(\xi, \theta, u), \quad (29)$$

$$y = H \xi + \delta h(\theta) u, \quad (30)$$

Let $v = \delta h(\theta) u$. The matrix $A_0 \in \mathbb{R}^n$ is deterministic and the matrix $\delta A(\theta) \in \mathbb{R}^n$ represents the uncertain part inherited from the uncertain nonlinear system (14)-(15). Symbol $b(\xi, \theta, u)$ indicates a lumped uncertain nonlinear function.

C. Bounding Functions and Interval Observers

The following assumptions will be used to facilitate the interval observer designs.

Assumption 2. $\underline{\delta A} \leq \delta A(\theta) \leq \overline{\delta A}$ for all $\theta \in \Theta$ and some known $\overline{\delta A}, \underline{\delta A} \in \mathbb{R}^{n \times n}$.

Assumption 3. $\underline{b}(t) \leq b(\xi, \theta, u) \leq \overline{b}(t)$, $|v(\theta, t)| \leq V$, for all $\theta \in \Theta$ and $t \geq 0$ and some known $\underline{b}, \overline{b} \in \mathcal{L}_\infty^n$ and $V > 0$.

Remark 1. Assumption 2 constrains the uncertain matrix δA to the interval $[\underline{\delta A}, \overline{\delta A}]$, where $\underline{\delta A}$ and $\overline{\delta A}$ can be directly computed using the knowledge of Θ in the case of a boxed set. In (30), the term $v = \delta h(\theta) u$ can be viewed as the measurement noise that has an upper bound V .

According to Assumption 2 and Lemma 1, for a vector variable $\xi \in \mathbb{R}^n$ and $\underline{\xi} \leq \xi \leq \overline{\xi}$ for some $\underline{\xi}, \overline{\xi} \in \mathbb{R}^n$, we can conclude that

$$\begin{aligned} & \underline{\delta A}^+ \underline{\xi}^+ - \overline{\delta A}^+ \underline{\xi}^- - \underline{\delta A}^- \overline{\xi}^+ + \overline{\delta A}^- \overline{\xi}^- \\ & \leq (\delta A) \xi \leq \\ & \overline{\delta A}^+ \underline{\xi}^+ - \underline{\delta A}^+ \underline{\xi}^- - \overline{\delta A}^- \underline{\xi}^+ + \underline{\delta A}^- \overline{\xi}^-. \end{aligned} \quad (31)$$

For any vector $L \in \mathbb{R}^n$, it is followed from (30) that $L(y - H\xi - v) \equiv 0$. Thus, (29) can be reformulated by adding a zero term to the right hand side as

$$\begin{aligned} \dot{\xi} &= A_0 \xi + \delta A(\theta) \xi + b(\xi, \theta, u) + L(y - H\xi - v) \\ &= \underbrace{(A_0 - LH)}_D \xi + \underbrace{\delta A(\theta) \xi + b(\xi, \theta, u) + Ly - Lv}_U. \end{aligned} \quad (32)$$

In the second equality of (32), the system consists of a deterministic linear part denoted by D and an uncertain part represented by U . Denote by $\overline{\xi}(t)$ and $\underline{\xi}(t)$ the upper and lower

bound estimates of the state $\xi(t)$, respectively. The essence and main steps of an interval observer design are summarized as follows:

- Select observer gain L such that the matrix $(A_0 - LH)$ is both Hurwitz and Metzler.
- In the dynamics of $\overline{\xi}$ and $\underline{\xi}$, the uncertain term U is replaced by its (deterministic) bounding functions \overline{U} and \underline{U} , where $\underline{U} \leq U \leq \overline{U}$ for all $\theta \in \Theta$ and $t \geq 0$.
- The system states $\overline{\xi}$ and $\underline{\xi}$ are initialized such that $\overline{\xi}(0) \geq \xi(0)$ and $\underline{\xi}(0) \leq \xi(0)$.

With that, the monotone system based interval observer structure is proposed as follows [36],

$$\begin{aligned} \dot{\overline{\xi}} &= (A_0 - \overline{LH}) \overline{\xi} + (\overline{\delta A}^+ \overline{\xi}^+ - \underline{\delta A}^+ \overline{\xi}^- - \overline{\delta A}^- \underline{\xi}^+ + \underline{\delta A}^- \overline{\xi}^-) \\ &+ \overline{b}(t) + \overline{L}y + |\overline{L}|V, \end{aligned} \quad (33)$$

$$\begin{aligned} \dot{\underline{\xi}} &= (A_0 - \underline{LH}) \underline{\xi} + (\underline{\delta A}^+ \underline{\xi}^+ - \overline{\delta A}^+ \underline{\xi}^- - \underline{\delta A}^- \overline{\xi}^+ + \overline{\delta A}^- \overline{\xi}^-) \\ &+ \underline{b}(t) + \underline{L}y - |\underline{L}|V. \end{aligned} \quad (34)$$

The following theorem provides a sufficient condition for stability and enclosure of the interval observer design.

Theorem 1 ([36]). *Let Assumptions 2 & 3 be satisfied and the matrices $(A_0 - \overline{LH})$ and $(A_0 - \underline{LH})$ are Hurwitz and Metzler. Then $\underline{\xi}(t) \leq \xi(t) \leq \overline{\xi}(t)$, $\forall t \geq 0$ is satisfied provided that $\underline{\xi}_0 \leq \xi_0 \leq \overline{\xi}_0$. Furthermore, if there exists $P \in \mathbb{R}^{2n \times 2n}$, $P = P^\top \succ 0$ and $\gamma > 0$ such that the following Riccati matrix inequality is verified*

$$G^\top P + PG + 2\gamma^{-2}P^2 + \gamma^2 \eta^2 Id_{2n} + Z^\top Z \prec 0, \quad (35)$$

where $\eta = 2n \|\overline{\delta A} - \underline{\delta A}\|_{\max}$, $Z \in \mathbb{R}^{s \times 2n}$, $0 < s \leq 2n$ and

$$G = \begin{bmatrix} A_0 - \underline{LH} + \underline{\delta A}^+ & -\underline{\delta A}^- \\ -\overline{\delta A}^- & A_0 - \overline{LH} + \overline{\delta A}^+ \end{bmatrix}, \quad (36)$$

then $\underline{\xi}, \overline{\xi} \in \mathcal{L}_\infty^n$. Moreover,

$$\underline{x} = \inf(\Phi^{-1}(\eta)), \quad \overline{x} = \sup(\Phi^{-1}(\eta)), \quad (37)$$

where $\eta \in [\underline{\xi}, \overline{\xi}]$.

The enclosure property, i.e. $\underline{\xi}(t) \leq \xi(t) \leq \overline{\xi}(t)$, $\forall t \geq 0$, is verified by examining the dynamics of estimation errors,

$$\dot{\overline{e}} = (A_0 - \overline{LH}) \overline{e} + (\overline{U} - U), \quad (38)$$

$$\dot{\underline{e}} = (A_0 - \underline{LH}) \underline{e} + (U - \underline{U}). \quad (39)$$

The monotone system property introduced in Section IV-A guarantees that $\overline{e}(t), \underline{e}(t) \geq 0$ for all $t \geq 0$ if the matrices $(A_0 - \underline{LH})$ and $(A_0 - \overline{LH})$ are Hurwitz and Metzler, given that $\overline{e}(0), \underline{e}(0) \geq 0$.

Remark 2. One of the crucial conditions to design an interval observer based on (32) is to select gains \overline{L} and \underline{L} such that the matrices $(A_0 - \overline{LH})$ and $(A_0 - \underline{LH})$ are Hurwitz and Metzler. However, as pointed out in [35], the Metzler condition is usually unfeasible for observability-based forms. If such observer gains may not be found, no interval observer could be designed based on the monotone system. In this unfortunate case, an extra coordinate transformation relying on solving a Sylvester equation can be used to overcome this issue [35].

The proof for Theorem 1 is omitted here. Interested readers may refer to Theorem 7 of [36] for more details. We translate this theory to battery pack state estimation next.

V. INTERVAL OBSERVER FOR BATTERY PACK

In this section, the interval observer design introduced in Section IV is applied to the Li-ion battery pack state estimation problem. We examine the case of a string of heterogeneous battery cells, shown in Fig. 2, with each cell modeled by ECMs with temperature and SOC-dependent electrical parameters. The objective here is to determine the guaranteed upper and lower bounds, $\bar{z}(t)$ and $\underline{z}(t)$, for SOCs in a string of battery cells in real time. Mathematically,

$$\underline{z}(t) \leq z_k(t) \leq \bar{z}(t), \quad \forall k \in \{1, 2, \dots, m\}, t \geq 0. \quad (40)$$

The lower bound on SOC $\underline{z}(t)$ must be considered in a pack for cell-level protection during discharge, while an upper bound on SOC $\bar{z}(t)$ plays a similar role when the battery is being charged. This is why both estimated SOC bounds are useful and necessary during regular battery operation.

One practical advantage of using an interval observer for a group of cells is its scalability. An interval observer, composed of only two dynamical systems, i.e., system (33)-(34), estimating upper and lower bounds for all unmeasured state trajectories, significantly reduces computation and design efforts. Due to cell heterogeneity, an interval observer constructs two trajectories that upper and lower bound all SOC trajectories, without dealing with the differential-algebraic nature of the circuit dynamics. It is also worth highlighting that the width/tightness of the estimated intervals is dependent on the magnitude of model uncertainties, and our knowledge of the uncertainties when selecting the bounding functions \bar{U} and \underline{U} .

A. Model Set-up

It is stressed again that the voltage and current of each cell on the string is measured, but only the maximum and minimum voltages at each time t are accessible to the BMS estimation algorithm (See Assumption 1). For a battery cell electrically modeled by an ECM given by system (1)-(3), let

$$\theta_k(t) = \begin{bmatrix} R_{1,k}(z_k, T_k) & R_{2,k}(z_k, T_k) & C_k(z_k, T_k) & Q_k \end{bmatrix} \in \Theta \subset \mathbb{R}^4, \quad (41)$$

so that Θ is a four-dimensional polytope. Ideally, a deterministic state observer could be proposed for the state estimation of the coupled nonlinear electro-thermal system (1)-(8). However, this approach is intractable due to the system nonlinearities like electro-thermal coupling, state-dependent parameters and nonlinear voltage output function. To counteract this issue, we suppress the electrical parameters' dependence on the internal states, and treat these parameters as model uncertainties with known upper and lower bounds. In particular, suppose that the following upper and lower bounds are imposed on the uncertain parameters,

$$\underline{\theta} \leq \theta_k(t) \leq \bar{\theta}, \quad \forall k \in \{1, 2, \dots, m\}, \quad (42)$$

where

$$\underline{\theta} = \begin{bmatrix} \underline{R}_1 & \underline{R}_2 & \underline{C} & \underline{Q} \end{bmatrix}, \quad \bar{\theta} = \begin{bmatrix} \bar{R}_1 & \bar{R}_2 & \bar{C} & \bar{Q} \end{bmatrix}. \quad (43)$$

These inequalities require the knowledge of the extreme values of model parameters in the battery string. The extreme values could be found in practice through offline parameter identification. For instance, the work in [40] identifies the values of resistances and capacitance under various SOC and temperature conditions and constructs a multi-dimensional matrix for such mappings, for an LiFePO₄/Graphite battery (LFP type). The extreme values for the state-dependent parameters can be taken as the maximum and minimum possible values of the mappings across all temperatures and all SOCs. Moreover, the objective is to design a robust interval observer, using these extreme parameter values and extreme real-time measurements, to determine the set of admissible values for cell SOC at each time instant, when the plant model is subject to bounded uncertainties in the model parameters and states' initial conditions.

Let $\tau_k = 1/(R_{2,k}C_k)$, which is associated with the time constant of the system, and consider a known nominal value $\tau_{k,0}$ such that $\tau_k = \tau_{k,0} + \delta\tau_k$, in which $\tau_{k,0}$ can be freely assigned by the designer. In this set-up, $\tau_{k,0}$ is a deterministic scalar and $\delta\tau_k$ represents the uncertain component. From (43), the constant upper and lower bounds of $\delta\tau_k$ can be computed as

$$\underline{\delta\tau} \leq \delta\tau_k \leq \bar{\delta\tau}, \quad \forall k \in \{1, 2, \dots, m\}, \quad (44)$$

where

$$\underline{\delta\tau} = \frac{1}{\bar{R}_2\bar{C}} - \tau_{k,0}, \quad \bar{\delta\tau} = \frac{1}{R_2C} - \tau_{k,0}. \quad (45)$$

To facilitate the SOC interval observer design for a string of cells, we start with the general single cell electrical system (1)-(3) for a random cell k , where $k \in \{1, 2, \dots, m\}$. Although model (1)-(3) is specific to each cell, we explore the fact that all cells are dominated by the same model structure (only with different parametric and initial condition features). The estimated SOC intervals account for all uncertainties associated with each cell k , and generate a feasible envelope to enclose all possible SOC trajectories in the pack. In particular, model (1)-(3) can thus be formulated in terms of the uncertain system (14)-(15), with

$$\dot{x}_k = f(x_k) + B(\theta_k)u + \delta f(x_k, \theta_k), \quad (46)$$

$$V_k = h(x_k) + \delta h(\theta_k)u, \quad (47)$$

where

$$\begin{aligned} x_k &= \begin{bmatrix} x_{1,k} \\ x_{2,k} \end{bmatrix} = \begin{bmatrix} z_k \\ V_{c,k} \end{bmatrix}, \\ f(x_k) &= \begin{bmatrix} 0 \\ -\tau_{k,0}x_{2,k} \end{bmatrix}, \quad \delta f(x_k, \theta_k) = \begin{bmatrix} 0 \\ -\delta\tau_k x_{2,k} \end{bmatrix}, \\ B(\theta_k) &= \begin{bmatrix} \frac{1}{C_k} \\ \frac{Q_k}{C_k} \end{bmatrix}, \quad u = I_k(t), \\ h(x_k) &= V_{oc}(x_{1,k}) + x_{2,k}, \quad \delta h(\theta_k) = R_{1,k}. \end{aligned} \quad (48)$$

The local observability matrix for the nominal system is then given by

$$\mathcal{O}(x_k) = \begin{bmatrix} dh(x_k) \\ dL_f h(x_k) \end{bmatrix} = \begin{bmatrix} \frac{dV_{oc}}{dx_{1,k}}(x_{1,k}) & 1 \\ 0 & -\tau_{k,0} \end{bmatrix}, \quad (49)$$

whose rank is 2 if and only if the first derivative of the OCV function with respect to SOC is non-zero around an equilibrium point $x_{1,k} = x_{1,e}$ and $\tau_{k,0} \neq 0$, i.e.,

$$\frac{dV_{oc}}{dx_1}(x_{1,e}) \neq 0, \quad \tau_{k,0} \neq 0, \quad (50)$$

which aligns with existing results on local observability for battery ECMs [3]. Hence, the coordinate transformation based on Lie algebra

$$\Phi(x_k) = \begin{bmatrix} \xi_{1,k} \\ \xi_{2,k} \end{bmatrix} = \begin{bmatrix} V_{oc}(x_{1,k}) + x_{2,k} \\ -\tau_{k,0}x_{2,k} \end{bmatrix} \quad (51)$$

transforms the system (14), (15), with (48) to the nonlinear parameter-varying system

$$\dot{\xi}_k = A_0 \xi_k + \delta A(\theta_k) \xi_k + b(\xi_k, \theta_k, u), \quad (52)$$

$$V_k = H \xi_k + \delta h(\theta_k, u), \quad (53)$$

with $\xi_k = [\xi_{1,k} \quad \xi_{2,k}]^\top \in \mathbb{R}^2$, and

$$A_0 = \begin{bmatrix} 0 & 1 \\ 0 & -\tau_{k,0} \end{bmatrix}, \quad \delta A(\theta_k) = \begin{bmatrix} 0 & \frac{\delta \tau_k}{\tau_{k,0}} \\ 0 & -\delta \tau_k \end{bmatrix},$$

$$b(\xi_k, \theta, u) = \begin{bmatrix} \frac{1}{Q_k} \varphi \left(\xi_{1,k} + \frac{1}{\tau_{k,0}} \xi_{2,k} \right) + \frac{1}{C_k} \\ -\frac{\tau_{k,0}}{C_k} \xi_{2,k} \end{bmatrix} I,$$

$$H = \begin{bmatrix} 1 & 0 \end{bmatrix}, \quad \delta h(\theta_k) = R_{1,k}, \quad (54)$$

where

$$\varphi(\cdot) = \frac{dV_{oc}}{dx_{1,k}} \left(V_{oc}^{-1}(\cdot) \right). \quad (55)$$

In the coordinate transformation (51), $x_{1,k}$ is the SOC for cell k and $x_{2,k}$ is the relaxation voltage from the $R_{2,k} - C_k$ circuit. From a physical point of view, the variable $\xi_{1,k}$ (whose unit is Volt) can be interpreted as the summation of cell open circuit potential and overpotentials, or equivalently the cell voltage excluding the ohmic voltage, whereas $\xi_{2,k}$ represents a scaled version of the $R_{2,k} - C_k$ voltage. The interval observer can be designed based on (52)-(55) utilizing Theorem 1. Subsequently, we will demonstrate the procedures for (i) selecting observer gains, and (ii) obtaining the bounding functions for the uncertain terms given by (54)-(55).

Remark 3. *The interval observer design in Theorem 1 demands an invertible coordinate transformation Φ . An inverse transformation based on (51) yields*

$$\Phi^{-1}(\xi_k) = \begin{bmatrix} x_{1,k} \\ x_{2,k} \end{bmatrix} = \begin{bmatrix} V_{oc}^{-1} \left(\xi_{1,k} + \frac{1}{\tau_{k,0}} \xi_{2,k} \right) \\ -\frac{1}{\tau_{k,0}} \xi_{2,k} \end{bmatrix}. \quad (56)$$

The inverse transformation is feasible provided that the open circuit voltage curve is invertible. Hence, the invertibility of the open circuit voltage plays key roles in both model local observability and the feasibility of interval estimates in the x_k domain.

Remark 4. *It is noteworthy to mention that the internally positive system (38)-(39) could admit diagonal and even linear Lyapunov functions [47], [49], which is an useful property in*

scaling up the interval observer method, especially when advanced battery models (e.g. full-order electrochemical models [50]) with a large number of states is adopted.

One of the existing strategies for battery pack modeling and estimation relies on the weakest and strongest cells as representatives of the pack dynamics [27], [28]. In this context, it may be argued that instead of utilizing interval observers, one can simply consider the cells with extreme voltages, perform SOC estimation, and designate it as the pack SOC. Nevertheless, it should be emphasized that when battery is under operation (e.g., subject to a dynamic charging/discharging current profile), such a practice to select the cells with the lowest/highest voltages will not always recover lowest/highest SOCs in a pack. As an example, we demonstrated a simulation study using a UDDS drive cycle for two heterogeneous cells with different initial SOC values connected in series in Fig. 4. As can be clearly observed, cell 2 SOC is greater than that of cell 1 at all times, but the voltage of cell 2 is not always the highest. This is a notable advantage of the interval observers compared against the conventional voltage-based characterization of battery packs.

B. Interval Observer Gain Selection

As stated in Theorem 1, the observer gains \bar{L} and \underline{L} need to be chosen such that the matrices $(A_0 - \bar{L}H)$ and $(A_0 - \underline{L}H)$ are Hurwitz and Metzler. Remark 2 also emphasizes that such observer gains do not always exist. We now examine a sufficient condition on the observer gains to fulfill this design requirement.

Proposition 1. *Let $L = [L_1 \quad L_2]^\top \in \mathbb{R}^2$. If $\tau_{k,0} > 0$, $L_2 \leq 0$, and $L_1 > -L_2/\tau_{k,0} \geq 0$, then the matrix $(A_0 - LH)$ is Hurwitz and Metzler.*

Proof. The matrix $(A_0 - LH)$ is computed as

$$(A_0 - LH) = \begin{bmatrix} -L_1 & 1 \\ -L_2 & -\tau_{k,0} \end{bmatrix}. \quad (57)$$

For the off-diagonal elements to be non-negative, we require $L_2 \leq 0$. In addition, the eigenvalues of the matrix $(A_0 - LH)$ can be obtained symbolically as

$$\lambda_1 = \frac{-L_1 - \tau_{k,0} - \sqrt{(L_1 + \tau_{k,0})^2 - 4L_2}}{2}, \quad (58)$$

$$\lambda_2 = \frac{-L_1 - \tau_{k,0} + \sqrt{(L_1 + \tau_{k,0})^2 - 4L_2}}{2}. \quad (59)$$

Since $L_2 \leq 0$, the term $\sqrt{(L_1 + \tau_{k,0})^2 - 4L_2}$ is guaranteed to be a positive real number regardless of the values of L_1 and $\tau_{k,0}$. Furthermore, since $\lambda_2 \geq \lambda_1$, then λ_1 is assured to be negative if $\lambda_2 < 0$, which is equivalent to

$$L_1 + \tau_{k,0} > \sqrt{(L_1 + \tau_{k,0})^2 - 4L_2}. \quad (60)$$

First, the left hand side of (60) must be greater than 0, which yields $L_1 > -\tau_{k,0}$. Squaring both sides of (60) results in $L_1 \tau_{k,0} > -L_2$. Now we consider two scenarios: (i) $\tau_{k,0} < 0$ and (ii) $\tau_{k,0} > 0$. Under (i), we have that $-\tau_{k,0} < L_1 < -L_2/\tau_{k,0}$, which is an invalid interval because $L_2 \leq 0$. On the

other hand, under (ii), we have $L_1 > \max\{-\tau_{k,0}, -L_2/\tau_{k,0}\} = -L_2/\tau_{k,0}$. \square

Thus, in light of Proposition 1 and (45), it is recommended to choose $\tau_{k,0}$ such that $0 < \tau_{k,0} \leq 1/(\bar{R}_2\bar{C})$, in order to have $\delta\tau_k \geq 0$ for all $k \in \{1, 2, \dots, m\}$ to ease the design of bounding functions, as illustrated in the next section.

Remark 5. In our case, based on the above analysis, it is possible to design observer gains L_1 and L_2 such that the matrix $(A_0 - LH)$ is Hurwitz and Metzler. Therefore, the coordinate transformation, introduced in Remark 2, which results in solving a Sylvester equation is not required.

C. Bounding Functions

This section provides detailed steps to determine the bounding functions towards the interval observer designs. In the case of battery ECM, the uncertain function U in (32) is represented by

$$U = \delta A(\theta)\xi_k + b(\xi_k, \theta) + LV_k - LR_{1,k}I, \quad (61)$$

with the respective terms given in (54). Under Assumption 2 and 3, we seek the analytic expressions of \bar{U} and \underline{U} by constructing the bounding functions of each term on the right hand side of (61).

According to Proposition 1, the fact that $\tau_{k,0} > 0$ yields

$$\bar{\delta A} = \begin{bmatrix} 0 & \frac{\delta\tau}{\tau_{k,0}} \\ 0 & -\delta\tau \end{bmatrix}, \quad \delta A = \begin{bmatrix} 0 & \frac{\delta\tau}{\tau_{k,0}} \\ 0 & -\delta\tau \end{bmatrix}. \quad (62)$$

For the second term at the right hand side of (61), $b(\xi_k, \theta)$, the upper and lower bounding functions are constructed based on the sign of the applied current. Function $\varphi(\cdot)$ is essentially the slope of the OCV-SOC curve, and we assume that the OCV is strictly monotonic with respect to SOC and the slope of the OCV curve is bounded, i.e., $\underline{\varphi} \leq \varphi(\cdot) \leq \bar{\varphi}$ with known $\bar{\varphi}$ and $\underline{\varphi}$. Hence, when $I(t) \geq 0$,

$$\bar{b} = \begin{bmatrix} \frac{1}{\bar{Q}}\bar{\varphi} + \frac{1}{\bar{C}} \\ -\frac{\tau_{k,0}}{\bar{C}} \end{bmatrix} I, \quad \underline{b} = \begin{bmatrix} \frac{1}{\bar{Q}}\underline{\varphi} + \frac{1}{\bar{C}} \\ -\frac{\tau_{k,0}}{\bar{C}} \end{bmatrix} I. \quad (63)$$

The bounding functions for the third term on the right hand side of (61), namely LV_k , is positioned based on the signs of L_1 and L_2 . In particular, since $V_k > 0$, we have $L_1\underline{y} \leq L_1y \leq L_1\bar{y}$ and $L_2\bar{y} \leq L_2y \leq L_2\underline{y}$. Similar strategy can be applied to determine the bounding functions for the last term of U .

D. Adaptive Bounding Functions

The aforementioned approach that utilizes the (constant) extreme values of the mappings between ECM model parameters and SOC/Temperature is conservative, because it explores the worst-case scenario of the intervals and the resultant estimates for the SOC bounds may be wide. To address this issue, in this section we present an adaptive bounding function selection framework in order to reduce the parametric uncertainties. Before we state the main results, the following assumption on the thermal model (4)-(7) is introduced.

Assumption 4. The relations between local ECM model parameters and local SOC and temperature are static and known, and are same across all cells. Mathematically, the following two conditions hold:

- The analytic expressions of $R_{1,k}$, $R_{2,k}$, C_k with respect to z_k and T_k , $k \in \{1, 2, \dots, m\}$, do not change.
- If $z_i = z_j$ and $T_i = T_j$ for all $i \neq j$, then $R_{1,i}(z_i, T_i) = R_{1,j}(z_j, T_j)$, $R_{2,i}(z_i, T_i) = R_{2,j}(z_j, T_j)$, and $C_i(z_i, T_i) = C_j(z_j, T_j)$.

Thermally, cell-to-cell variations are dominated by

- Cell thermal parameter heterogeneity, i.e., $R_{c,i} \neq R_{c,j}$, $R_{u,i} \neq R_{u,j}$, $C_{c,i} \neq C_{c,j}$, and $C_{s,i} \neq C_{s,j}$, for all $i \neq j$.
- Cell heat generation heterogeneity. In particular, differences in cell resistances, voltages, and SOCs create distinct levels of heat generation, thus promote different temperature trajectories across cells.

Therefore, the interval observer for the thermal component of the string can be realized by treating heat generation rate as an exogenous input whose upper and lower bounds are inherited from the estimated SOC intervals. The thermal interval observer seeks to determine the guaranteed bounds, $\bar{T}(t)$ and $\underline{T}(t)$, for all cell temperature trajectories in the battery string in an online fashion, subject to uncertain model parameters and heat generations. Namely, $\underline{T}(t) \leq T_k(t) \leq \bar{T}(t)$ for all $k \in \{1, 2, \dots, m\}$ and $t \geq 0$. For a battery cell k thermally modeled by the interconnected system (4)-(7), let

$$\theta_{T,k} = \begin{bmatrix} R_{c,k} & R_{u,k} & C_{c,k} & C_{s,k} \end{bmatrix}. \quad (64)$$

We further assume that $\theta_{T,k}$ is upper and lower bounded for all $k \in \{1, 2, \dots, m\}$ by $\underline{\theta}_T \leq \theta_{T,k}(t) \leq \bar{\theta}_T$ where

$$\underline{\theta}_T = \begin{bmatrix} \underline{R}_c & \underline{R}_u & \underline{C}_c & \underline{C}_s \end{bmatrix}, \quad \bar{\theta}_T = \begin{bmatrix} \bar{R}_c & \bar{R}_u & \bar{C}_c & \bar{C}_s \end{bmatrix}. \quad (65)$$

Note that the cell thermal model (4)-(7) is itself in the partial linear form. Thus, it can be directly written in the form of the partial-linear expression (29)-(30) with $\xi_{T,k} = [T_{c,k} \quad T_{s,k}]^\top$:

$$\begin{aligned} \dot{\xi}_{T,k} &= A_{T,k}\xi_{T,k} + b_{T,k}(t) \\ &= A_{T,0}\xi_{T,k} + \delta A_{T,k}(\theta_{T,k})\xi_{T,k} + b_{T,k}(t), \end{aligned} \quad (66)$$

$$y_{T,k} = H_T\xi_{T,k} + \delta h_T(\theta_{T,k})u, \quad (67)$$

where $\delta A_{T,k} = A_{T,k} - A_{T,0}$. Suppose that the nominal values for the thermal parameters are $\theta_{T,0} = [R_{c,0} \quad R_{u,0} \quad C_{c,0} \quad C_{s,0}]$, the compact matrices in (66)-(67) are given by

$$\begin{aligned} A_{T,k} &= \begin{bmatrix} -\frac{1}{R_{c,k}C_{c,k}} & \frac{1}{R_{c,k}C_{c,k}} \\ \frac{1}{R_{c,k}C_{s,k}} & -\left(\frac{1}{R_{u,k}C_{s,k}} + \frac{1}{R_{c,k}C_{s,k}} + \frac{2}{R_{cc}C_{s,k}}\right) \end{bmatrix}, \\ A_{T,0} &= \begin{bmatrix} -\frac{1}{R_{c,0}C_{c,0}} & \frac{1}{R_{c,0}C_{c,0}} \\ \frac{1}{R_{c,0}C_{s,0}} & -\left(\frac{1}{R_{u,0}C_{s,0}} + \frac{1}{R_{c,0}C_{s,0}} + \frac{2}{R_{cc}C_{s,0}}\right) \end{bmatrix}, \\ b_{T,k} &= \left[\frac{1}{C_{c,k}}\dot{q}_k \quad \frac{1}{R_{u,k}C_{s,k}}T_f + \frac{1}{R_{cc}C_{s,k}}(T_{s,k+1} + T_{s,k-1}) \right]^\top, \\ H_T &= \begin{bmatrix} 0 & 1 \end{bmatrix}, \quad \delta h_T = 0. \end{aligned} \quad (68)$$

It is noted that the pair $(A_{T,0}, H_T)$ is observable. Ultimately, in light of the thermal system (66)-(67), three major sources of uncertainties are considered in the thermal interval observer

design: (i) the heat generation rate \dot{q}_k as an uncertain exogenous input, (ii) the parametric uncertainty $\delta A_{T,k}$ in (66), which is assumed to be upper and lower bounded and the bounds are known, and finally (iii) the measurement uncertainty on the surface temperatures due to communication bus limitations (see Assumption 1). In particular, the first one translates to nominating a set of bounding functions for $b_{T,k}$ such that $\underline{b}_T \leq b_{T,k} \leq \bar{b}_T$ for all $k \in \{1, 2, \dots, m\}$. Since the current $I_k(t)$ is measured, the extreme values of voltage (V_{\max} and V_{\min}) are accessible, and the upper and lower bounds of $z_k(t)$ are acquired from the ECM interval observer, the bounding functions can be updated in real time using these quantities. As an illustrative example, when current is positive ($I_k > 0$), we have

$$\bar{b}_T = \left[I_k(V_{\max} - V_{oc}(\underline{z})) \quad \frac{1}{R_u C_s} T_f + \frac{2}{R_{cc} C_s} \bar{T} \right]^\top, \quad (69)$$

$$\underline{b}_T = \left[\max\{0, I_k(V_{\min} - V_{oc}(\bar{z}))\} \quad \frac{1}{R_u C_s} T_f + \frac{2}{R_{cc} C_s} \underline{T} \right]^\top. \quad (70)$$

Theorem 1 can now be applied to the system (66)-(67) for estimating the temperature upper and lower intervals of all cells in the pack. The details are omitted here as the procedures are similar to that in Section V-A and V-B.

At this moment, we are positioned to state our proposed scheme for achieving the adaptive bounding function selection in the design of the interval observer, which is depicted in Fig. 5. The ECM-based interval observer block (purple) receives the extreme values of cell voltages and the present upper and lower bounds on the ECM model parameters across all cells, and produces a guaranteed upper and lower bounds for all SOC trajectories of the battery string, \bar{z} and \underline{z} . Next the thermal-based interval observer (salmon) seeks to achieve guaranteed upper and lower bounds on all temperature conditions in real time by using the upstream SOC intervals as well as the extreme values of surface temperature measurements. The crucial part of this framework is highlighted by mapping the state (SOC and temperature) intervals to the parameter intervals $\bar{\theta}(t)$ and $\underline{\theta}(t)$ in real time (green), by taking advantages of Assumption 4. Herein, rather than using the worst-case ECM parameter values in the pack (see (43)) which yields conservative interval estimates (will be demonstrated in Section VI), the bounds on the uncertain parameters are updated simultaneously based on the current state interval estimates, rendering an improved knowledge on the model parametric uncertainties. Consequently, the updated bounds on the ECM parameters act as feedback signals and in turn facilitate the ECM-based interval observer design with a tighter interval estimates.

VI. SIMULATION STUDIES

In order to numerically validate the interval observer designs, in this section, we present results from simulations to evaluate the performance of the proposed interval observer for battery strings. The simulations are carried out on battery cells with 2.8 Ah nominal capacity modeled by the lumped electro-thermal model (1)-(8). The state-dependent electrical model parameters are taken from [40], and the nominal values for the thermal parameters are given by

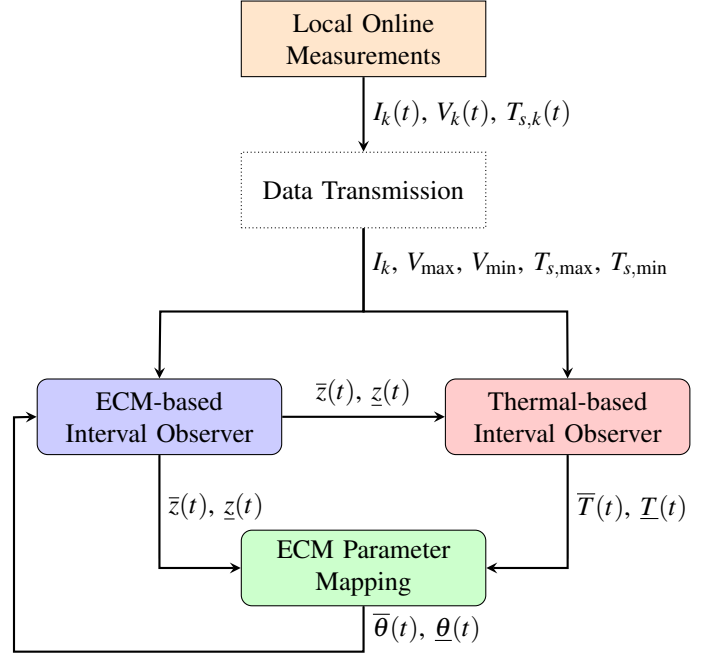


Fig. 5. Interval observer framework for battery cells connected in series with adaptive bounding functions.

$\theta_{T,0} = [1.94 \text{ K/W} \quad 15 \text{ K/W} \quad 62.7 \text{ J/K} \quad 4.5 \text{ J/K}]$. To evaluate the interval observer performance under dynamical loads, the current applied to the battery pack is an appropriately scaled UDDS drive cycle, shown in Fig 6(a). We examine a series arrangement of five heterogeneous cells, i.e., $m = 5$ in Fig. 2. In the plant model, to imitate the SOC imbalance, the cells are initialized with different SOC levels, and Fig. 6(b) records the voltage response of each cell. **Moreover, we intentionally perturb the thermal parameters of each cell by at most 10% from the nominal values to produce thermal heterogeneity (see Table I).** In addition, suppose the cells are thermally simulated from heterogeneous initial temperatures, whereas the ambient environment is kept at room temperature ($T_f = 25^\circ \text{C}$). Under this scenario, the lumped temperature of each cell is reported in Fig. 6(c).

The interval observer from Theorem 1 is utilized to estimate the feasible SOC and temperature intervals from only current, max/min voltages, and max/min surface temperature measurements. For all presented simulations, the upper and lower interval estimates must be initialized at points that are higher and lower than all initial conditions in the plant model, respectively. Two scenarios are demonstrated. First, the interval observer without the adaptive bounding functions is tested (Section V-C). Then, the results are expected to improve with an adaptive bounding function (Section V-D).

A. Bounding Function with No Adaptation

Let us first evaluate the effectiveness of the SOC interval observer using bounding functions with no thermal adaptation. The initial values on the SOC interval observers (lower and upper bounds) are 14% and 49%. The observer gains are chosen to be $\underline{L} = [10 \quad -0.1]^\top$ and $\bar{L} = [10 \quad -0.1]^\top$, which

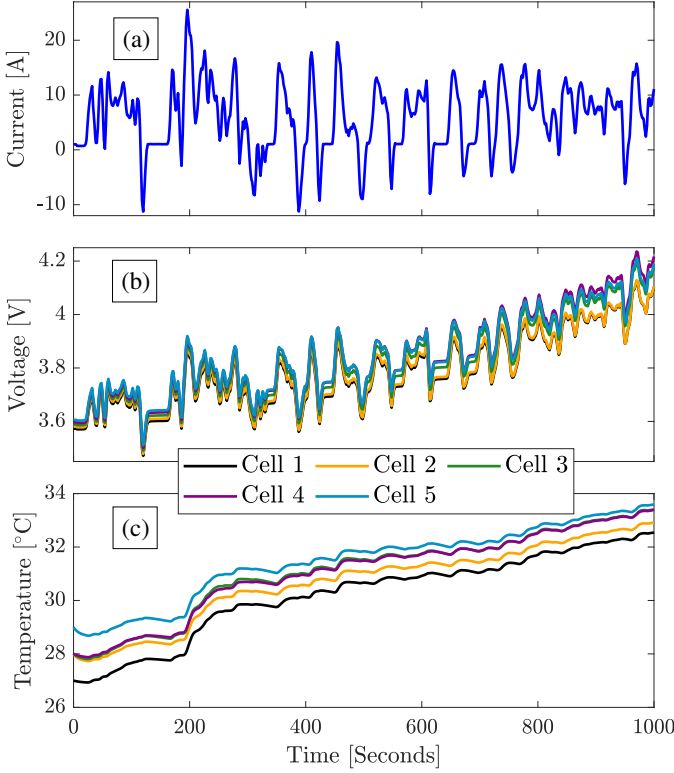


Fig. 6. The simulated plant model for a string of five heterogeneous cells under an UDDS profile. The cells are initialized to different SOC/voltage and temperature values. All cells have the same thermal model parameters. (a) input current; (b) voltage; (c) temperature.

TABLE I
ELECTRO-THERMAL MODEL PARAMETERS

	$z_k(0)$	$T_k(0)$	Q_k	$R_{c,k}$	$R_{u,k}$	$C_{c,k}$	$C_{s,k}$
Cell 1	28%	27	2.8	1.8	13.9	66.6	4.1
Cell 2	30%	28	2.9	2.1	14.8	67.8	4.3
Cell 3	32%	28	2.7	2.1	16.2	58.0	4.5
Cell 4	34%	28	2.65	1.9	15.9	67.9	4.9
Cell 5	36%	29	2.85	2.0	16.4	64.4	4.9
Unit	[-]	°C	Ah	K/W	K/W	J/K	J/K

ensure that $(A_0 - LH)$ and $(A_0 - \bar{L}H)$ are Metzler and Hurwitz. From Fig. 6(c), the temperature range of the pack under the UDDS drive cycle is approximately between 25 °C and 35 °C. Thus, the maximum and minimum ECM parameter values within this range are extracted to form the constant electrical parameter bounds $\bar{\theta}$ and $\underline{\theta}$ (see (42)-(43)). In this case, Fig. 7(a) plots the simulated SOC temporal evolution of five cells (colored solid lines) and the corresponding estimated SOC upper and lower intervals (dashed lines). Ultimately, the intervals recover instantly from large initial errors and always enclose the true SOC of the string at all times. These results confirm the stability and inclusion properties of the designed interval observer stated in Theorem 1, given uncertain initial conditions and state-dependent electrical parameters.

However, the assumption on the exact knowledge of the

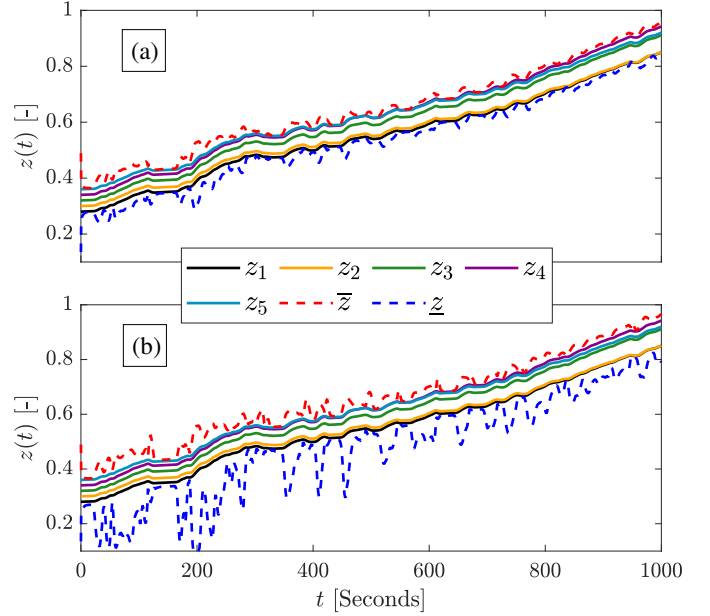


Fig. 7. The interval observer performance for five heterogeneous cells in series, without adaptive bounding functions. The tightness of the estimated SOC intervals increases with better knowledge on the parameter uncertainties. (a) interval estimation under adequate knowledge of model parametric uncertainties; (b) interval estimation when the parametric uncertainties are large.

temperature range is hardly predictable in practice. Fig. 7(b) investigates the interval observer performance with a weaker awareness of the temperature evolution. Unlike the previous case, the parameter mapping with a wider range of temperatures are involved such that the constant parameter bounds $\bar{\theta}$ and $\underline{\theta}$ become more conservative. As can be expected, the estimated SOC intervals produce highly noticeable estimation errors. This is indeed our practical motivation to study the bounding functions with thermal adaptation. Furthermore, note the spikes on the estimated intervals in Fig. 7(b). These spikes are in alignment with the spikes on the input current profile shown in Fig. 6(a). Essentially, the large current magnitudes magnify the uncertainties of the model in places where it is mathematically multiplied by an uncertain parameter, e.g., see the last term on the right hand side of (53). Ultimately, the interval observers for battery pack application are highly sensitive to high currents, so it is imperative to reduce the effects of large currents that potentially amplify system uncertainties, via smart bounding function selections.

B. Bounding Function with Adaptation

Now we consider the interval observer design with adaptive bounding functions. The design procedures follow the framework presented in Fig. 5. This method simultaneously estimates the SOC intervals and temperature intervals using Theorem 1, and updates the upper and lower bounds of the uncertain parameters according to the present state intervals. Consequently, the numerical results are delineated in Fig. 8. The solid curves represent the simulated state trajectories of each cell in the plant model, and the dashed lines denote the feasible SOC and temperature bounds for the string of

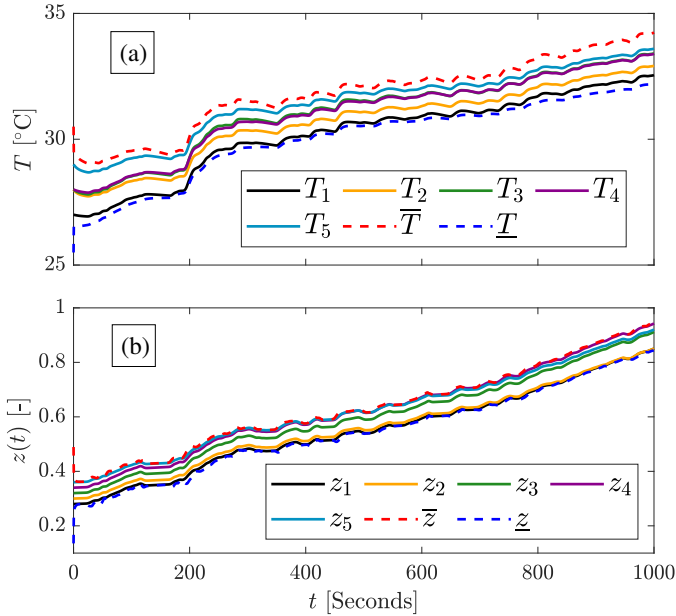


Fig. 8. The interval observer performance for five heterogeneous cells in series, with adaptive bounding functions. The estimated SOC intervals significantly outperforms the ones from Fig. 7. (a) temperature interval observer; (b) SOC interval observer.

TABLE II
SOC INTERVAL ESTIMATION TIGHTNESS COMPARISON

Scenarios	SOC Upper RMSE	SOC Lower RMSE
Case 1 (Fig. 7a)	2.34%	2.09%
Case 2 (Fig. 7b)	3.49%	8.94%
Case 3 (Fig. 8b)	0.85%	1.11%

cells. It should be emphasized that these results are produced under the same settings that were used to generate Fig. 7(b). Comparing Fig. 8(b) and 7(b), the SOC/temperature intervals computed with adaptive bounding functions effectively reduce the estimation errors induced by the conservative bounds on the uncertain parameters.

The root mean squared error (RMSE) between SOC intervals and the real SOC trajectories are enumerated in Table II to quantitatively evaluate the interval tightness. Specifically in Table II, SOC upper RMSE indicates the RMSE between the upper interval and the maximum SOC trajectory, whereas SOC lower RMSE computes the RMSE between the lower interval and the minimum SOC. Unsurprisingly, Case 3, in which the bounding functions are adapted according to the present SOC and temperature intervals, provides significantly lower RMSE values for both upper and lower intervals compared to Case 2.

C. Comparison with EKF

Finally, the proposed interval observer for a battery pack with cells connected in series is compared against the state-of-the-art single cell observer, i.e., the extended Kalman filter (EKF). We implement an EKF on each individual cell in the battery string to estimate its local SOC, using local

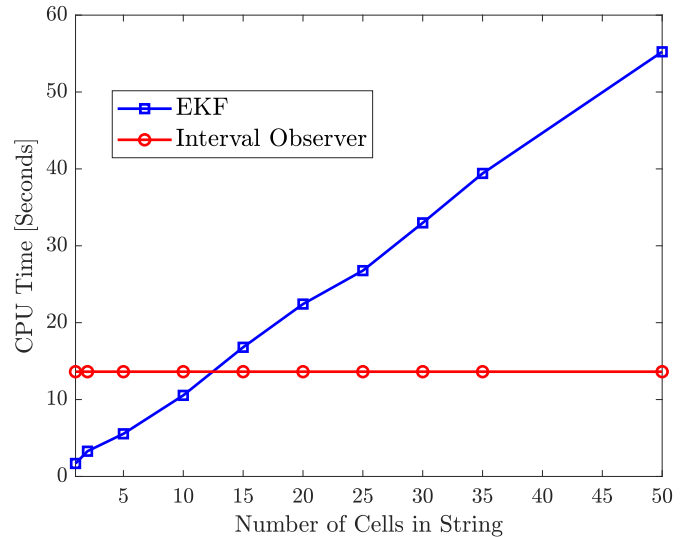


Fig. 9. CPU time of an interval observer compared with CPU time of an EKF. The interval observer is independent of the number of cells thus requiring a constant CPU time. The time consumed by single cell-based EKF increases linearly with cell number.

voltage and current measurements. Note that an EKF requires accurate local cell model parameters and local measurements for SOC estimation, whereas the interval observer only needs maximum and minimum values of voltage and temperature among all cells. **To the best of the authors' knowledge, most of current on-board battery management systems for large-scale applications, e.g. EVs, idealize battery packs by lumping the cells together and defining a pack-level SOC. For few of those who attempt to extract cell-level SOC information in battery packs, Coulomb counting with voltage re-calibration is the primary adopted strategy given its structural and computational simplicity. Ultimately, although EKF for individual cells in a pack is computationally heavy and generally not seen in the on-board EV battery management systems nowadays, they are largely considered as one of the most advanced embedded algorithms for state estimation in future BMS's owing to its robustness to uncertainties and self-correcting nature.** Fig. 9 compares the CPU times of i) running an EKF for each cell with 2) running an interval observer for the entire string, with respect to the number of cells in the string. These results are produced with an Intel i7 2.2GHz processor with 16GB RAM. The CPU time consumed by executing an EKF for individual cell SOC estimation grows almost linearly with increasing number of cells. That is, in a battery pack composed of hundreds or thousands of cells, having a large amount of real-time local estimators would demand a high computational power. In contrast, regardless of the number of cells, an interval observer only consumes a fixed CPU time since it consistently solves only four dynamical equations, i.e., two for SOC and two for temperature, to return the feasible intervals. Consequently, although the interval observers may not account for individual SOC information in a battery pack, it escalates algorithm scalability and considerably reduces computation and design complexities. Finally, it is noteworthy that the estimated intervals can be treated as the worst-case and best-

case scenarios for battery pack internal states, which are crucial for potential extended study of control/stabilization of battery packs [51], [52].

VII. CONCLUSIONS

An interval observer based on an equivalent circuit-thermal model for lithium-ion battery packs has been presented in this paper. The SOC-temperature-dependent parameters are considered as unknown but bounded uncertainties. Then, a series arrangement of cells is used for observer design, where cell heterogeneity is now accounted for through the uncertainty bounding functions. Given that the nominal battery model is locally observable, the original uncertain model can be transformed into a partial-linear form, which enables interval estimation based on monotone systems. By properly choosing the observer gains, the state matrix of the estimation error is Hurwitz and Metzler, which guarantees stability and inclusion of the state bound estimates. Further, the bounding functions can be adapted based on the present estimated SOC and temperature intervals to enhance the tightness of the bounds. A major feature of the proposed estimation approach is its scalability, since the number of states of interval observers is independent of the number of cells. The computational effort required by an interval observer for a pack is significantly lower than that of a single cell-based EKF, as demonstrated by simulations.

REFERENCES

- [1] Michael A Roscher, Oliver S Bohlen, and Dirk Uwe Sauer. Reliable state estimation of multicell lithium-ion battery systems. *IEEE Transactions on Energy Conversion*, 26(3):737–743, 2011.
- [2] Kandler Smith and Chao-Yang Wang. Power and thermal characterization of a lithium-ion battery pack for hybrid-electric vehicles. *Journal of power sources*, 160(1):662–673, 2006.
- [3] Shi Zhao, Stephen R Duncan, and David A Howey. Observability analysis and state estimation of lithium-ion batteries in the presence of sensor biases. *IEEE Transactions on Control Systems Technology*, 25(1):326–333, 2016.
- [4] Nalin A Chaturvedi, Reinhardt Klein, Jake Christensen, Jasim Ahmed, and Aleksandar Kojic. Algorithms for advanced battery-management systems. *IEEE Control systems magazine*, 30(3):49–68, 2010.
- [5] Scott J Moura, Federico Bribiesca Argomedo, Reinhardt Klein, Anahita Mirtabatabaei, and Miroslav Krstic. Battery state estimation for a single particle model with electrolyte dynamics. *IEEE Transactions on Control Systems Technology*, 25(2):453–468, 2016.
- [6] Dong Zhang, Satadru Dey, Luis D Couto, and Scott J Moura. Battery adaptive observer for a single-particle model with intercalation-induced stress. *IEEE transactions on control systems technology*, 2019.
- [7] Reinhardt Klein, Nalin A Chaturvedi, Jake Christensen, Jasim Ahmed, Rolf Findeisen, and Aleksandar Kojic. Electrochemical model based observer design for a lithium-ion battery. *IEEE Transactions on Control Systems Technology*, 21(2):289–301, 2012.
- [8] Dong Zhang, Luis D Couto, and Scott J Moura. Electrode-level state estimation in lithium-ion batteries via kalman decomposition. *IEEE Control Systems Letters*, 5(5):1657–1662, 2020.
- [9] Xiaosong Hu, Shengbo Li, and Hui Peng. A comparative study of equivalent circuit models for Li-ion batteries. *Journal of Power Sources*, 198:359–367, 2012.
- [10] Y Hu and S Yurkovich. Battery cell state-of-charge estimation using linear parameter varying system techniques. *Journal of Power Sources*, 198:338–350, 2012.
- [11] Dong Zhang, Satadru Dey, Hector E Perez, and Scott J Moura. Remaining useful life estimation of lithium-ion batteries based on thermal dynamics. In *American Control Conference (ACC)*, pages 4042–4047, 2017.
- [12] IL-Song Kim. A technique for estimating the state of health of lithium batteries through a dual-sliding-mode observer. *IEEE Transactions on Power Electronics*, 25(4):1013–1022, 2009.
- [13] Akram Eddahech, Olivier Briat, Eric Woirdard, and Jean-Michel Vinassa. Remaining useful life prediction of lithium batteries in calendar ageing for automotive applications. *Microelectronics Reliability*, 52(9-10):2438–2442, 2012.
- [14] Saehong Park, Dong Zhang, and Scott Moura. Hybrid electrochemical modeling with recurrent neural networks for Li-ion batteries. In *American Control Conference (ACC)*, pages 3777–3782, 2017.
- [15] Freeman Rufus, Seungkoo Lee, and Ash Thakker. Health monitoring algorithms for space application batteries. In *International Conference on Prognostics and Health Management*, pages 1–8, 2008.
- [16] Scott J Moura, Miroslav Krstic, and Nalin A Chaturvedi. Adaptive PDE observer for battery SOC/SOH estimation. In *Dynamic Systems and Control Conference*, volume 45295, pages 101–110. American Society of Mechanical Engineers, 2012.
- [17] Satadru Dey, Beshah Ayalew, and Pierluigi Pisu. Nonlinear robust observers for state-of-charge estimation of lithium-ion cells based on a reduced electrochemical model. *IEEE Transactions on Control Systems Technology*, 23(5):1935–1942, 2015.
- [18] Saeed Sepasi, Reza Ghorbani, and Bor Yann Liaw. A novel on-board state-of-charge estimation method for aged Li-ion batteries based on model adaptive extended Kalman filter. *Journal of Power Sources*, 245:337–344, 01 2014.
- [19] Qingsong Wang, Ping Ping, Xuejuan Zhao, Guanquan Chu, Jinhua Sun, and Chunhua Chen. Thermal runaway caused fire and explosion of lithium ion battery. *Journal of Power Sources*, 208:210–224, 2012.
- [20] John Wang, Ping Liu, Jocelyn Hicks-Garner, Elena Sherman, Souren Soukiazian, Mark Verbrugge, Harshad Tataria, James Musser, and Peter Finamore. Cycle-life model for graphite-LiFePO₄ cells. *Journal of Power Sources*, 196(8):3942–3948, 2011.
- [21] Michel Broussely, Ph Biensan, F Bonhomme, Ph Blanchard, S Herreyre, K Nechev, and RJ Staniewicz. Main aging mechanisms in Li ion batteries. *Journal of Power Sources*, 146(1-2):90–96, 2005.
- [22] Tarun Huria, Massimo Ceraolo, Javier Gazzarri, and Robyn Jackey. High fidelity electrical model with thermal dependence for characterization and simulation of high power lithium battery cells. *IEEE International Electric Vehicle Conference (IEVC)*, 2012.
- [23] Xinfan Lin, Hector E Perez, Jason B Siegel, Anna G Stefanopoulou, Yonghua Li, R Dyche Anderson, Yi Ding, and Matthew P Castanier. On-line parameterization of lumped thermal dynamics in cylindrical lithium ion batteries for core temperature estimation and health monitoring. *IEEE Transactions on Control Systems Technology*, 21(5):1745–1755, 2012.
- [24] Xinfan Lin, Hector Perez, Jason Siegel, Anna Stefanopoulou, Yi Ding, and Matthew Castanier. Parameterization and observability analysis of scalable battery clusters for onboard thermal management. *Oil & Gas Science and Technology*, 68(1):165–178, 2013.
- [25] S. Castano, L. Gauchia, E. Voncila, and J. Sanz. Dynamical modeling procedure of a Li-ion battery pack suitable for real-time applications. *Energy Conversion and Management*, 92:396–405, 2015.
- [26] Dong Zhang, Luis D Couto, Sebastien Benjamin, Wenteng Zeng, Daniel F Coutinho, and Scott J Moura. State of charge estimation of parallel connected battery cells via descriptor system theory. In *2020 American Control Conference (ACC)*, pages 2207–2212. IEEE, 2020.
- [27] Liang Zhong, Chenbin Zhang, Yao He, and Zonghai Chen. A method for the estimation of the battery pack state of charge based on in-pack cells uniformity analysis. *Applied Energy*, 113:558–564, 2014.
- [28] Yin Hua, Andrea Cordoba-Arenas, Nicholas Warner, and Giorgio Rizzoni. A multi time-scale state-of-charge and state-of-health estimation framework using nonlinear predictive filter for lithium-ion battery pack with passive balance control. *Journal of Power Sources*, 280:293–312, 2015.
- [29] Yuejiu Zheng, Minggao Ouyang, Languang Lu, Jianqiu Li, Xuebing Han, Liangfei Xu, Hongbin Ma, Thomas A. Dollmeyer, and Vincent Freyermuth. Cell state-of-charge inconsistency estimation for LiFePO₄ battery pack in hybrid electric vehicles using mean-difference model. *Applied Energy*, 111:571–580, 2013.
- [30] Xu Zhang, Yujie Wang, Duo Yang, and Zonghai Chen. An on-line estimation of battery pack parameters and state-of-charge using dual filters based on pack model. *Energy*, 115:219–229, 2016.
- [31] Xiaosong Hu, Fengchun Sun, and Yuan Zou. Estimation of state of charge of a lithium-ion battery pack for electric vehicles using an adaptive Luenberger observer. *Energies*, 3(9):1586–1603, 2010.

- [32] Gregory Plett. Extended Kalman filtering for battery management systems of LiPB-based HEV battery packs: Part 1. Background. *Journal of Power Sources*, 134:252–261, 2004.
- [33] Luis D Couto and Michel Kinnaert. Partition-based unscented Kalman filter for reconfigurable battery pack state estimation using an electrochemical model. In *American Control Conference (ACC)*, pages 3122–3128, 2018.
- [34] Taesic Kim, Wei Qiao, and Liayn Qu. Online SOC and SOH estimation for multicell lithium-ion batteries based on an adaptive hybrid battery model and sliding-mode observer. In *IEEE Energy Conversion Congress and Exposition*, pages 292–298, 2013.
- [35] Tarek Raïssi, Denis Efimov, and Ali Zolghadri. Interval state estimation for a class of nonlinear systems. *IEEE Transactions on Automatic Control*, 57(1):260–265, 2011.
- [36] Stanislav Chebotarev, Denis Efimov, Tarek Raïssi, and Ali Zolghadri. Interval observers for continuous-time LPV systems with L1/L2 performance. *Automatica*, 58:82–89, 2015.
- [37] Gang Zheng, Denis Efimov, and Wilfrid Perruquetti. Design of interval observer for a class of uncertain unobservable nonlinear systems. *Automatica*, 63:167–174, 2016.
- [38] Hector E Perez and Scott J Moura. Sensitivity-based interval PDE observer for battery SOC estimation. In *American Control Conference (ACC)*, pages 323–328, 2015.
- [39] Dong Zhang, Luis D Couto, Preet Gill, Sebastien Benjamin, Wentu Zeng, and Scott J Moura. Interval observer for SOC estimation in parallel-connected lithium-ion batteries. In *2020 American Control Conference (ACC)*, pages 1149–1154. IEEE, 2020.
- [40] Xinfan Lin, Hector E Perez, Shankar Mohan, Jason B Siegel, Anna G Stefanopoulou, Yi Ding, and Matthew P Castanier. A lumped-parameter electro-thermal model for cylindrical batteries. *Journal of Power Sources*, 257:1–11, 2014.
- [41] Xinfan Lin, Yi Ding, Matthew P Castanier, and Anna G Stefanopoulou. Estimating core temperatures of battery cells in a battery pack, March 12 2019. US Patent 10,230,137.
- [42] Dong Zhang, Satadru Dey, Hector E Perez, and Scott J Moura. Real-time capacity estimation of lithium-ion batteries utilizing thermal dynamics. *IEEE Transactions on Control Systems Technology*, 2019.
- [43] Xinfan Lin, Anna G Stefanopoulou, Yonghua Li, and R Dyche Anderson. State of charge estimation of cells in series connection by using only the total voltage measurement. In *2013 American Control Conference*, pages 704–709. IEEE, 2013.
- [44] Thorsten Baumhöfer, Manuel Brühl, Susanne Rothgang, and Dirk Uwe Sauer. Production caused variation in capacity aging trend and correlation to initial cell performance. *Journal of Power Sources*, 247:332–338, 2014.
- [45] Michael Baumann, Leo Wildfeuer, Stephan Rohr, and Markus Lienkamp. Parameter variations within li-ion battery packs—theoretical investigations and experimental quantification. *Journal of Energy Storage*, 18:295–307, 2018.
- [46] Hal L Smith. Monotone dynamical systems: an introduction to the theory of competitive and cooperative systems. *Bulletin (New Series) of the American Mathematical Society*, 33:203–209, 1996.
- [47] Lorenzo Farina and Sergio Rinaldi. *Positive linear systems: theory and applications*, volume 50. John Wiley & Sons, 2011.
- [48] Alberto Isidori. *Nonlinear control systems*. Springer Science & Business Media, 2013.
- [49] Yoshio Ebihara, Dimitri Peaucelle, and Denis Arzelier. LMI approach to linear positive system analysis and synthesis. *Systems & Control Letters*, 63:50–56, 2014.
- [50] Karen E Thomas, John Newman, and Robert M Darling. Mathematical modeling of lithium batteries. In *Advances in lithium-ion batteries*, pages 345–392. Springer, 2002.
- [51] Denis Efimov, Tarek Raïssi, and Ali Zolghadri. Control of nonlinear and LPV systems: interval observer-based framework. *IEEE Transactions on Automatic Control*, 58(3):773–778, 2013.
- [52] Denis Efimov, Andrey Polyakov, and Jean-Pierre Richard. Interval observer design for estimation and control of time-delay descriptor systems. *European Journal of Control*, 23:26–35, 2015.